JACS
JOURNAL OF THE AMERICAN CHEMICAL SOCIETY
Article
Cite This: J. Am. Chem. Soc. 2019, 141, 10109−10116
pubs.acs.org/JACS

Potential-Induced High-Conductance Transport Pathways through Single-Molecule Junctions

Parisa Yasini,[†,§] Sepideh Afsari,[†,§] Haowei Peng,[‡,§] Piret Pikma,[†] John P. Perdew,[†,‡] and Eric Borguet*[,†]

[†]Department of Chemistry and [‡]Department of Physics, Temple University, Philadelphia, Pennsylvania 19122, United States

Supporting Information

ABSTRACT: Employing single molecules as electronic circuit building blocks is one promising approach to electronic device miniaturization. We report single-molecule junction formation where the orientation of molecules can be controlled externally by the working electrode potential. The scanning tunneling microscopy break junction (STM-BJ) method is used to bridge tetrafluoroterephthalic acid (TFTPA) and terephthalic acid (TPA) molecules between the Au(111) electrode and the STM tip to measure the single-molecule conductance through the junction. When the Au(111) electrode is at negative potentials (with respect to the zero-charge potential), a highly ordered and flat-oriented superstructure forms, allowing for direct contact between the π system of the benzene ring of the molecules and the Au(111) electrode, leading to junction formation with no anchoring group involvement. Our first-principles nonequilibrium Green's function (NEGF) computation shows a flat configuration yields a conductance that is 3 orders of magnitude larger than for a molecule vertically connected to the electrodes via anchoring groups. Conductances of 0.24 ± 0.04 and 0.22 ± 0.02 G_0 are experimentally measured with the flat configurations of TFTPA and TPA, respectively. These values are at least 2 orders of magnitude higher than the experimental values previously reported for the conductance of TPA bridged through carboxylic acid anchoring groups (3.8×10^{-4}–3.2×10^{-3} G_0). In contrast, a positively charged surface triggers an order−disorder transition eliminating the high-conductance states, most likely because the formation of the flat-oriented junction is prevented. The dependence of TFTPA conductance on the electrode potential (electrode Fermi level) suggests a LUMO mediated transport mechanism. Calculation confirms the lack of an effect of the addition of an electron-withdrawing group are investigated.

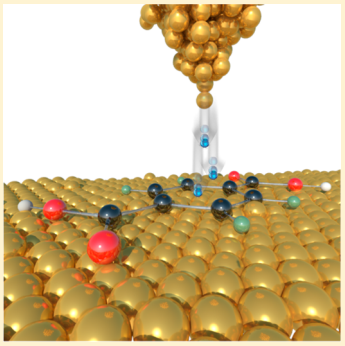

INTRODUCTION

Single molecules can potentially be employed as building blocks for miniaturized electronic devices.[1,2] Understanding and controlling the architecture of the single-molecule junctions are essential steps in fabricating such building blocks. To this end, the scanning tunneling microscopy-based break junction (STM-BJ) method has been widely used to study charge transport through single-molecule junctions by wiring a single molecule in the nanoscale gap created between the STM tip and the substrate. STM can image the possible long-range-ordered molecular adlayers, thereby providing information as to the probable orientation of the molecule in the junction. The formation of the ordered molecular network and the orientation of molecules can be controlled through applying potential to the substrate (electrode) as an external stimulus to induce an order−disorder transition in the adsorbed molecules. In such systems, the external potential can further tune the relative energy of the electrode Fermi level with respect to the frontier orbitals (MOs) of the adsorbed molecule[3−5] and hence can regulate the charge transport through the single-molecule junction.[6]

When electron transport in a single molecule is dominated by a tunneling mechanism, as is frequently the case, the current through the molecule can be defined as

$$I(V) = \frac{2e}{h} \int T(E)(f_l(E) - f_r(E))\, dE \quad (1)$$

where h is Planck's constant, e is the electron charge, $T(E)$ is the transmission of the molecular junction, and $f_l(E)$ and $f_r(E)$ are the Fermi functions for the electrons in the left and right electrodes, respectively.[7] The transmission $T(E)$ at the left and right electrodes and consequently the current in eq 1 depend on the nature of the contacts between the electrodes and the molecule.[8,9]

In a typical single-molecule junction, the molecule−electrode contacts are made through anchoring groups which are essential to stabilizing the junction by forming chemical bonds between the electrodes and the molecule. However, the anchoring groups can also act as a resistive component, blocking the transmission and lowering the conductance. In this study, we investigate the charge transport through potential-induced flat-oriented single molecules. In this scenario, hybridization of the delocalized π system of the benzene ring with the metal density of states enables charge-transport measurement perpendicular to the benzene ring,[10,11]

Received: May 21, 2019
Published: June 17, 2019

DOI: 10.1021/jacs.9b05448
J. Am. Chem. Soc. 2019, 141, 10109−10116

suppressing the resistive effect of conventional anchoring groups such as thiols and amines, leading to highly conductive single-molecule junctions. In our previous study, the conductance of a single mesitylene molecule was measured through direct contact between the gold electrodes and the π-system of the conjugated mesitylene ring under ambient conditions and was found to be 0.125 ± 0.006 G_0.[12] Previous studies have shown that measuring conductance perpendicular to the benzene ring results in high conductance values[13−16] while the conductance of other single benzene derivatives connected to the electrodes by anchoring groups is at least 1 order of magnitude lower (typically 10^{-2}−10^{-4} G_0).[17−22]

In the present work, using a combination of electrochemical STM (EC-STM) and STM-BJ methods as well as a first-principles nonequilibrium Green's function (NEGF) computation, we report the measurement of charge transport through single tetrafluoroterephthalic acid (TFTPA) and terephthalic acid (TPA) molecules adsorbed with the benzene ring oriented flat on a charged Au(111) electrode (Figure 1a). TFTPA and

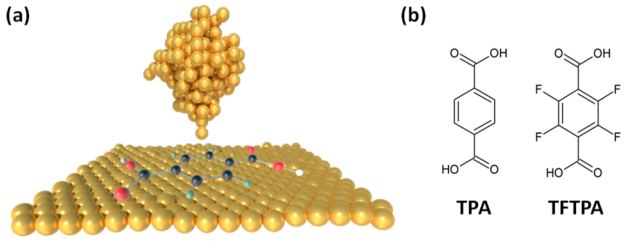

Figure 1. Schematic of the orientation-controlled single-molecule junction and TPA and TFTPA structures. (a) Schematic of the TFTPA configuration in direct π-binding between the Au tip and the Au(111) substrate (electrode). (b) TPA and TFTPA molecular structures.

TPA (Figure 1b) belong to the family of small aromatic molecules with carboxylic acid functional groups capable of forming intermolecular hydrogen bonds which can lead to large ordered-structure domains on Au(111). The adsorption geometry of TFTPA and TPA molecules on the gold surface can be controlled using the electrode potential, allowing charge transport to be measured along a specific axis of the molecule as determined by the orientation of the molecule in the junction. Ultimately, surface-potential-controlled orientation and conductance could be a convenient strategy for designing single-molecule switches.

RESULTS AND DISCUSSION

EC-STM and Cyclic Voltammetry (CV) of TFTPA. The STM images and CV show that the order/disorder transition and the associated control of molecular orientation can be achieved through electrode potential modulation. The negatively charged electrode supports an ordered network of flat-lying molecules, while the molecules are disordered and likely vertically oriented[23,24] on the positively charged electrode. Our EC-STM images show the first successful in situ STM imaging of long-range-ordered domains of TFTPA molecules in an electrochemical environment under potential control (Figure 2a). A closer look at the zoomed-in STM images along with cross-sectional analysis in different directions reveals that the dimension of observed features on the surface is consistent with the estimated size of TFTPA (~0.7 nm × ~0.5 nm), suggesting that the benzene rings of the TFTPA molecules are arranged parallel to the negatively charged surface in a pattern of long lateral stripes on the gold electrode (Figure 2b and S2).

The adsorption of TFTPA and the formation of ordered structures are facilitated by two factors. First, Au(111) is negatively charged, driving the adsorption of TFTPA through interactions with the delocalized π-electron system as is commonly observed for aromatic molecules.[23,25] The appearance of the herringbone reconstruction pattern on the negatively charged gold surface can be easily observed (Figure 2b), suggesting physisorption (weak electrode−molecule interaction) of TFTPA on the electrode and limited charge transfer, consistent with the CV discussed later.[26] Second, hydrogen bond formation between carboxylic acid functional groups of TFTPA and donor−acceptor fluorine−fluorine interactions provides attractive forces[27,28] (Figure S2) promoting the formation of an ordered supramolecular structure of TFTPA on gold. Sweeping the electrode potential to values more positive than the zero-charge potential of the bare Au(111) ($0.32V_{SCE}$ for the reconstructed Au(111)-(22 × $\sqrt{3}$) and $0.23V_{SCE}$ for Au(111)-(1 × 1))[29] triggers an order−disorder transition (Figure 2c), as carboxylic acid groups might become deprotonated and incapable of forming hydrogen bonds.[23] Therefore, the molecular layer is not ordered as the bare Au(111), gold islands, and disordered layer can be observed at positive potentials.(Figure 2c).

Cyclic voltammetry (CV) supports the observed dynamics of surface reconstruction and the adsorbed molecules (e.g., possible phase transitions of the molecular adlayer as the electrode potential changes).[30] The CV of Au(111)/H_2SO_4 and TFTPA/Au(111)/H_2SO_4, recorded in the STM cell with platinum reference and counter electrodes in a potential range where no oxidation or reduction process occurs, shows multiple features (Figure 2e). Peaks P_1 (cathodic) and P'_1 (anodic) observed in the CV of Au(111) at 0.2 V_{SCE} (the potential referenced to the saturated calomel electrode) can be ascribed to the transition between the (22 × $\sqrt{3}$) reconstruction and the (1 × 1) unreconstructed phase of Au(111) (Figure 2e, dashed line).[31] These peaks are highly sensitive to the orientation and the quality of the single-crystal surface. Once the reconstruction is lifted, the sulfate ions start to adsorb, resulting in a sharp peak at around 0.8 V_{SCE}. The appearance of this reversible peak indicates that the surface is free of contamination.[32] As the electrode potential is swept back to more negative values, the herringbone reconstruction starts to recover (P'_1) but is not as complete as in the first scan because the recovery of the herringbone reconstruction is a diffusion-controlled process and it takes time to be completed.[29,33,34] The CV of TFTPA/Au(111) (Figure 2e, solid line) shows cathodic/anodic peaks P_2/ P'_2 at around 0.4 V_{SCE}, consistent with the reversible order/disorder transition of TFTPA on the gold surface. The appearance of P_1 and P'_1 implies that the adsorption of TFTPA on Au(111) does not lift the reconstruction (consistent with Figure 2a, discussed before) and there is little charge transfer between the molecule and the electrode.

EC Single-Molecule Conductance (SMC) Measurements of TFTPA. The single-molecule conductance measurements of TFTPA were carried out using the STM break junction method in solution under surface potential control in the current range of 0−10000 nA (details in Supporting Information, Figure S1), and more than 3000 current−distance curves were recorded. Close examination of the data reveals

DOI: 10.1021/jacs.9b05448
J. Am. Chem. Soc. 2019, 141, 10109−10116

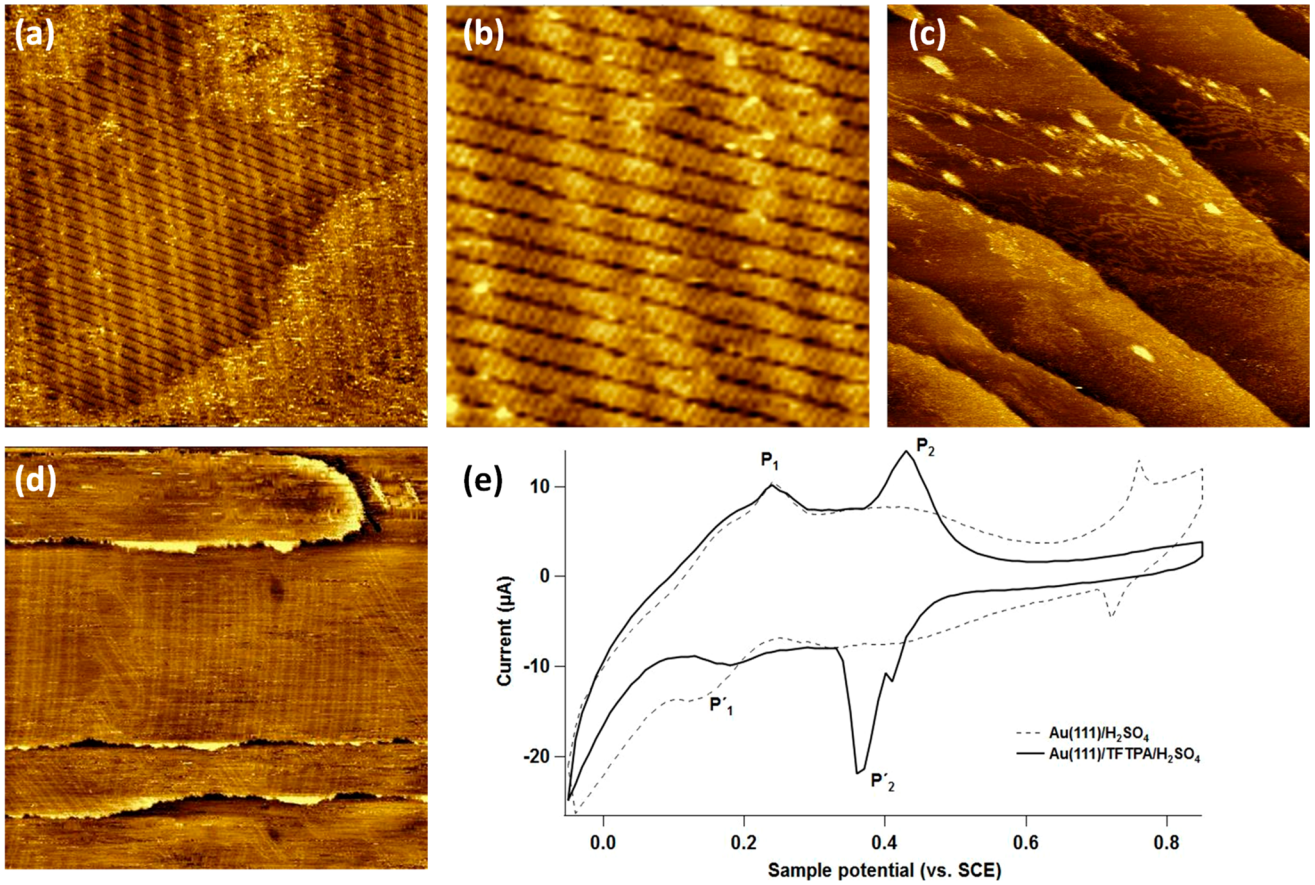

Figure 2. STM images and cyclic voltammetry of the TFTPA order−disorder transition: (a) STM images of TFTPA/0.05 M H_2SO_4 on Au(111) at V_S = 0 V_{SCE}, V_{bias} = −0.03 V, scan area 60 × 60 nm^2. (b) Scan area = 15 × 15 nm^2. (c) V_S = 0.65 V_{SCE}, V_{bias} = 0.06 V, scan area 100 × 100 nm^2. (d) STM image of bare Au(111)/0.05 M H_2SO_4 at V_S = 0 V_{SCE}, V_{bias} = −0.03 V, scan area 100 × 100 nm^2. (e) Cyclic voltammograms of a freshly prepared, flame-annealed bare Au(111) electrode in 0.05 M H_2SO_4 aqueous electrolyte (dashed line) and 0.1 mM TFTPA in 0.05 M H_2SO_4 aqueous electrolyte (solid line). The potential sweep rate was 100 $mV{\cdot}s^{-1}$. All images were acquired at I_t = 0.1 nA.

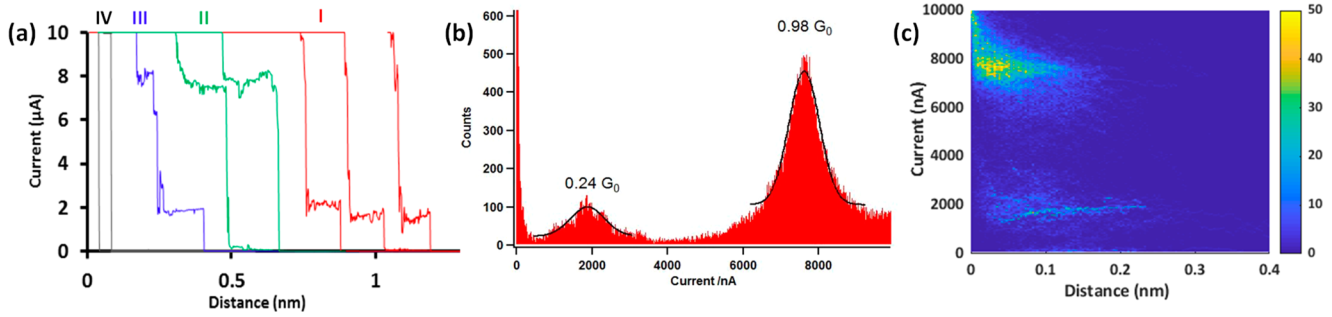

Figure 3. Sample STM-BJ data and the current histogram showing TFTPA and gold−gold junctions. (a) Typical individual current−distance curves collected in 0.05 M H_2SO_4 at V_S = 0 V_{SCE} and V_{bias} = 0.10 V attributed to molecular junctions (red, type I), gold junctions (green, type II), molecular junctions and gold junctions (blue, type III), and empty junctions (gray, type IV). (b) One-dimensional current histogram measured in 0.05 M H_2SO_4 with 0.1 mM TFTPA at V_S = 0 V_{SCE} and V_{bias} = 0.10 V. The solid line is a Gaussian profile used to accurately determine the peak positions (black). (c) Two-dimensional current−distance histogram plotted using the same number of curves as for the 1D current histogram. The histograms in b and c are based on 615 curves out of 3075 recorded.

that there are four types of current−distance curves (Figure 3a). Some traces showed clear single steps at around 1.8 μA (type I) and 7.75 μA (type II) corresponding to the molecular junction and the gold−gold atomic junction (quantum of conductance: $G_0 = 2e^2/h$ = 7.75× 10^{-5} S characteristic of single gold atom wires[35]), respectively. Some of the curves show two steps (type III), suggesting both molecular and atomic gold junctions. The rest of the curves, the vast majority (~80%), were simple exponential decays suggesting unsuccessful molecular junction formation (type IV).

To find the most probable conductance of the single-molecule junction, 1D and 2D current histograms were constructed. A data selection procedure was applied to all current−distance curves so that only stepped traces with a step length longer than 100 pm were used to construct current histograms to determine the molecular conductance (details in Supporting Information, Figure S3). The constructed histo-

DOI: 10.1021/jacs.9b05448
J. Am. Chem. Soc. 2019, 141, 10109−10116

gram (Figure 3b) contains two well-defined peaks at 0.24 ± 0.04 and 0.98 ± 0.03 G_0. The error bars represent the standard deviation of the conductance values determined in five different experiments. We attribute the 0.24 G_0 to charge transport through the benzene ring of TFTPA lying flat on the surface.

STM-BJ experiments with different biases showed that the observed conductance is bias-independent (details in Supporting Information, Figure S4) and represents the conductance of TFTPA. The 0.98 G_0 peak corresponds to charge transport through the Au−Au junction.[36]

The assignment of the 0.24 G_0 feature to a molecular junction due to the hybridization of the delocalized π system of the molecular orbitals with the metal density of states is supported by the immobilization of TFTPA in a flat orientation in the molecular network observed by the STM images. During the break junction process, the tip approaches the surface gradually (with an approach rate ranging from 0.016 to 0.025 $\mu m \cdot s^{-1}$) until it reaches a maximum current of 10 000 nA. Therefore, the tip does not go far beyond the formation of a single Au−Au junction (~77 500 nA at 0.1 V_{bias}). Consequently, we anticipate a relatively gentle and nondestructive contact of the tip with the surface and molecules, prompting the formation of a local perturbation. Depending on tip and instrument conditions, the tip moves laterally ~5 to 6 nm between approach−retract curves and will typically not land back on the disturbed areas; details are provided in the Supporting Information, Figure S10. In addition, because molecules are ordered as a result of strong intermolecular hydrogen bonding and metal−π interactions between the benzene ring and the electrode, the molecules do not behave as free molecules on the surface. In spite of tip-induced changes, their orientation will recover quickly to the initial low-energy state. Hence, we believe that the observed flat-oriented TFTPA molecules remain flat during the break junction process. Ultimately, this orientation leads to high coupling between the molecule and the electrodes, leading to a decreased junction length and associated resistance. This high-conductance peak (0.24 G_0) disappeared at a positive electrode potential (V_s = 0.65 V_{SCE}), where no ordered structure or flat-oriented molecules were observed, demonstrating that under these conditions no molecular junction formed with TFTPA in the flat configuration (Figure S 5d).

It is worth mentioning that this simplified model does not consider that the molecule's geometry in the junction might deviate from the ideal flat configuration due to the possibility that the gold surface is not atomically flat everywhere. However, the 2D histograms exhibit two clear features with length on the order of 0.2 nm assigned to the gold junction and the molecular junction. The length of the molecular junction is consistent with the flat-oriented molecules forming junctions without anchoring group participation, supporting junction formation through the π system of the flat-oriented benzene ring of the molecule on the surface. Even if the molecule is slightly tilted and not perfectly flat, the typical junction length is still on the order of 0.2 nm. Therefore, it appears that deviations from the flat geometry are not significant and the reported high conductance is associated with a quasi-flat configuration.

To determine the dominant molecular orbital in the tunneling process, we performed a series of STM-BJ experiments on TFTPA at different electrode potentials. The results (Figure 4 with details in Supporting Information, Figure S5) showed that as the Au electrode potential becomes more positive, the conductance value of TFTPA decreases, suggesting that the Fermi level of the gold electrodes is moving away from the conductance-mediating molecular orbitals of TFTPA.[37] This points to the LUMO as a major channel and mediating orbital in charge transport through single TFTPA molecules (Figure 4). According to the analysis of junction length based on 2D histograms (Figure S5 insets), the length of the molecular junctions did not change while the electrode potential swept to V_s = 0.35 V_{SCE}, exhibiting a stable, flat orientation on the surface. However, the high-conductance peak and the molecular junction feature associated with the flat orientation were not observed at V_S = 0.65 V_{SCE}, consistent with the lack of ordered structure in the STM images at positive electrode potentials.

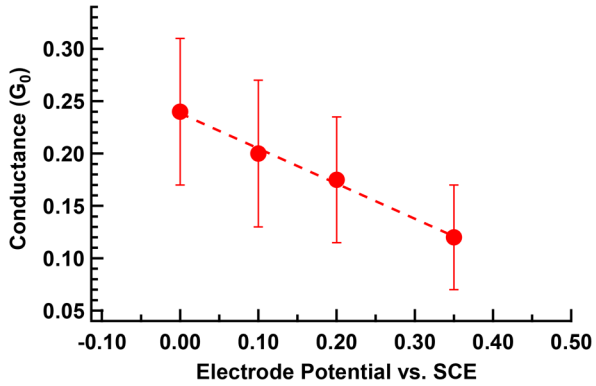

Figure 4. TFTPA conductance vs electrode potential. Linear fitting is shown with dashed line. Error bars are the full half-width maximum (FHWM) of each peak as it appeared in the conductance histograms (Figure S5) constructed at different electrode potentials.

As a control and in order to investigate the possibility of junction formation in other orientations forming less-conductive junctions, we measured current−distance curves of TFTPA molecule in negative (V_s = 0 V_{SCE}) and positive (V_s = 0.65 V_{SCE}) electrode potentials in the lower current range. Constructed current histograms at negative potential (Figure S9a) did not show any well-defined peak corresponding to the charge transport through molecular junctions, consistent with our hypothesis that the flat orientation of the molecule on the surface at negative potentials resulted in high-conductance junctions. Single-molecule conductance at positive surface potential, where molecules might be adsorbed randomly on the surface, did not show well-defined peaks either (Figure S9b). This could be due to the random orientations of TFTPA at the positive electrode potential, resulting in a lack of well-defined single-molecule junction formation.

EC-STM and SMC Measurements of TPA. The electronic structure of the molecule may have a considerable effect on molecule energy levels and charge transport through molecular junctions.[38−41] Specifically, it is generally accepted that the nonresonant charge transport mechanism depends on the height of the tunneling barrier and the relative alignment of the highest occupied molecular orbital (HOMO) and the lowest unoccupied molecular orbital (LUMO) with the Fermi level.[40,42] Previous studies have shown that the HOMO−LUMO gap, their energy alignment relative to the Fermi level, and subsequent charge transport through anchoring-group-terminating molecules in the junction can be manipulated using chemical substituents.[43] However, the effect of the

DOI: 10.1021/jacs.9b05448
J. Am. Chem. Soc. 2019, 141, 10109−10116

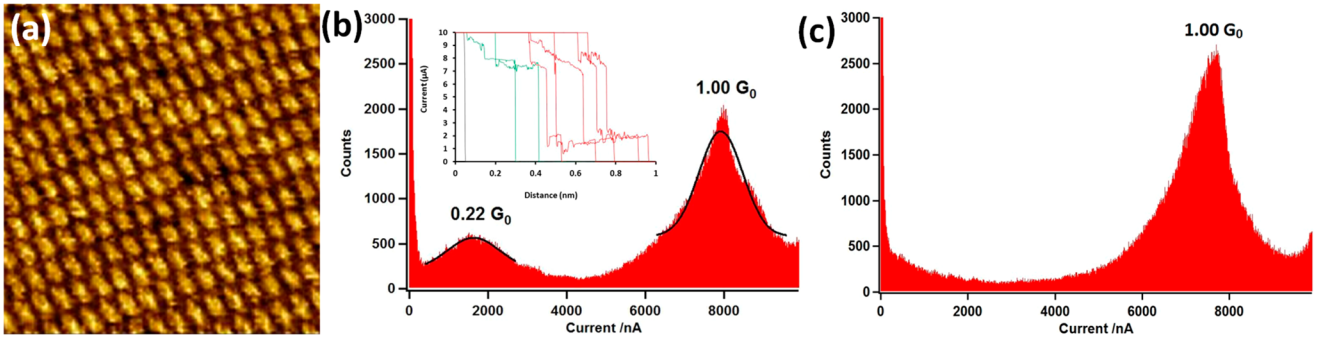

Figure 5. STM image and conductance histograms of TPA measured at negative and positive electrode potentials. (a) STM image of TPA/0.05 M H_2SO_4 on Au(111) at V_S = −0.10 V_{SCE}, scan area 10 × 10 nm^2. (b, c) All-data-point EC-STM-BJ current histograms of TPA collected on the Au(111) electrode without any data selection at (b) V_S = 0 V_{SCE}. (c) V_S = 70 V_{SCE}. V_{bias} = −0.1 V for both (b) and (c). (b-Inset) Example of individual current−distance traces collected on negatively charged Au(111). Gray: No atomic/molecular junction formed, Green: gold junctions. Red: gold and molecular junctions.

substitution group on the energy alignment of molecular orbitals and the charge transport perpendicular to the molecular plane have not yet been addressed.

To provide conclusive experimental evidence that we measured the conductance via direct Au−π contact and to study the effect of chemical substituents on the molecular orbital alignment and charge transport through the benzene ring, we performed a series of measurements for TPA which (Figure 1b) has two carboxylic acid groups and, similar to TFTPA, forms a long-range-ordered adlayer with the benzene ring lying flat on the negatively charged Au(111).[44] Our high-resolution STM images indicate linear stripes (Figure 5a) formed by planar-oriented TPA molecules aligning end to end with hydrogen bonds between the carboxylic groups (details in Supporting Information, Figure S6). Histograms of the SMC measurements on the negatively charged Au(111) in the presence of the planar-oriented TPA ordered structure reveal a conductance peak at 0.22 ± 0.02 G_0 (Figure 5b) that is at least 2 orders of magnitude higher than the experimental values reported in the literature for TPA, presumably anchored in the junction via its carboxylic acid groups.[22,45] However, the high-conductance peak (0.22 G_0) disappeared at positive electrode potentials (Figure 5c) where the molecular adlayer was disordered, suggesting that no molecular junctions formed with TPA in the flat configuration under these conditions. Two-dimensional histograms of TPA at negative electrode potential (Figure S7a) show clear features with length on the order of 0.2 nm consistent with flat-oriented molecules and the junction formation through π system of the flat-oriented benzene ring of the molecule on the surface.

These results confirm that the high-conductance peaks (0.24 and 0.22 G_0 for TFTPA and TPA, respectively) are repeatedly observed for two different benzenecarboxylic derivatives under conditions that provide the planar orientation of the benzene rings on the gold substrate, where the most likely charge transport path between the two gold electrodes is perpendicular to the benzene ring.[12] Thus, it seems that (i) the 0.24 and 0.22 G_0 conductance peaks are due to conductivity perpendicular to the benzene ring and (ii) our experimental results, confirmed by calculations discussed below, show that the substitution of hydrogen atoms of the benzene ring in TPA with strong electron-withdrawing groups (fluorine atoms) does not appear to significantly change the alignment of the dominant conductance channel (LUMO) of TFTPA in its flat orientation; hence the conductance of flat-oriented TFTPA remained unaffected relative to that of TPA. Furthermore, it is noteworthy to mention that, because of the hydrogen bonding between flat-oriented molecules, each single molecule is influenced by the hydrogen bond interactions and experiences a different physical and electronic environment relative to that of the isolated molecule. Hence, the reported conductance of flat-oriented TFTPA and TPA could be somewhat different from that of isolated TFTPA and TPA single molecules.[46]

Configuration Dependence of Charge Transport from First-Principles NEGF Computation. The significant difference between the conductance of TPA measured for the vertical and flat configurations[45] suggests dramatic changes in the junction electronic structure with the orientation of the molecule, which can be examined with first-principles calculations. The results are shown in Figure 6, and the computational details including the structure modeling are referred to in the Supporting Information. The value of the zero-bias transmission at the Fermi energy, E_F, provides a good estimation of the low-bias conductance measurement (eq 1)). TPA and TFTPA junctions with the same configuration have similar conductance (Figure 6a), while the difference in conductance between the flat and vertical configurations is as large as 3 orders of magnitude (TPA-flat, 0.31 G_0; TPA-vertical, 0.6 × 10^{-3} G_0; TFTPA-flat, 0.29 G_0; TFTPA-vertical, 0.3 × 10^{-3} G_0).

This dramatic contrast emphasizes the junction geometry effects, which can be intuitively attributed to the existence of anchoring groups for the vertical configuration as a scattering source as well as the much longer transport pathway. From the isosurface plots of the local density of states (LDOS) around the molecule near the Fermi energy, we clearly see the LDOS delocalized over the whole TFTPA molecule for the flat configuration (Figure 6b) while strongly localized near the anchoring group for the vertical configuration (Figure 6c). (The LDOS isosurface plots for TPA are very similar to those of TFTPA and therefore not shown here.) The computation confirms the junction configuration itself as a good conductance-controlling parameter for such benzene derivatives.

Potential Dependence from First-Principles NEGF. To mimic and rationalize the effects of the electrode potential (shift in the Fermi level of the electrodes) on the single-molecule conductance of TFTPA in the experiments, we applied a gate voltage in the area of the molecule[47,48] during the NEGF computation. Different from the experimental

DOI: 10.1021/jacs.9b05448
J. Am. Chem. Soc. 2019, 141, 10109−10116

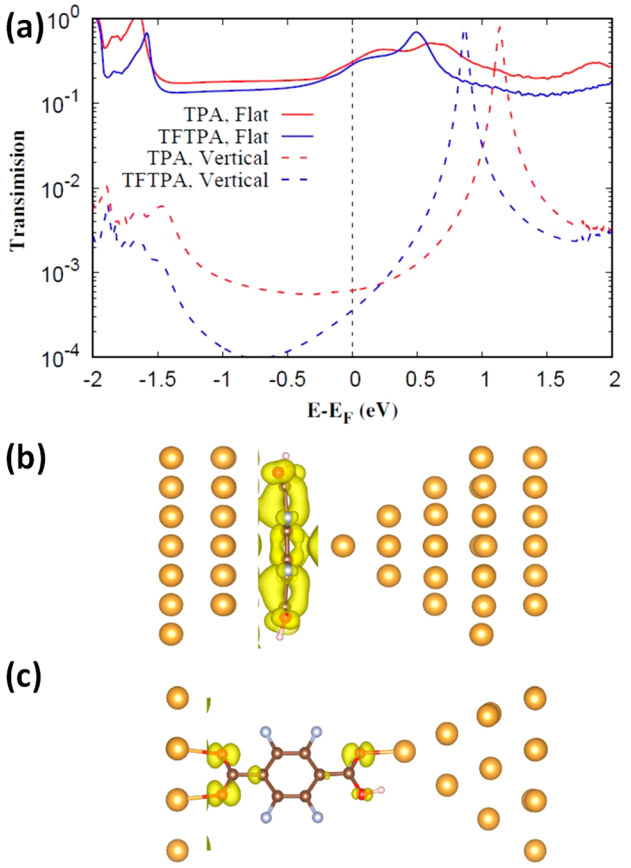

Figure 6. (a) Calculated zero-bias transmission spectra for TPA and TFTPA between gold electrodes with the flat and vertical configurations and the isosurface plot for the local density of states (LDOS) near the Fermi level for the TFTPA junction with (b) flat and (c) vertical configurations. For clarity, only the isosurface near the molecule and only parts of the structural models are shown in (b) and (c).

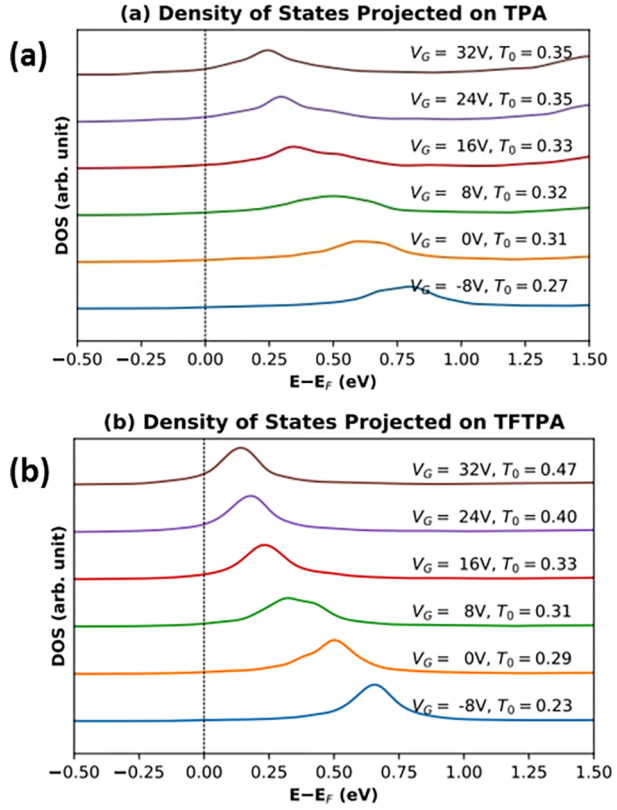

Figure 7. Projected density of states (DOS) of the molecules under different gate voltages for (a) TPA and (b) TFTPA. The DOSs are vertically shifted for clarification, and the corresponding gate voltages and transmission at the Fermi level are explicitly denoted.

setting, which modifies the potential of the electrodes to adjust the position of the electrode Fermi level, here we apply an electrostatic potential within the box which contains the molecule, and hence we mainly modify the energy position of the molecular orbitals. Both approaches should lead to the same effects of changing the relative energy difference between the Fermi level and the frontier orbitals of TFTPA and TPA. Note that a very large electrostatic potential is needed because of the screening effects.[48]

The peaks of the projected density of states (PDOS) corresponding to the LUMO are at 0.6 eV for TPA and 0.5 eV for TFTPA above the Fermi level under zero gate voltage (Figure 7). The HOMO-like states are about 1.6 eV below the Fermi level, which are not shown in the figure. The TFTPA LUMO peak is closer to the Fermi level and is generally narrower than that of TPA. The latter may arise from the ∼0.2 Å longer separation between the tip and the surface in the case of TFTPA and hence a weaker coupling between TFTPA and the electrodes. These two factors could explain the very similar conductance between the two molecules.

In agreement with experiment (Figure 4), the calculations (Figure 7) show that when the energy difference between the LUMO and the Fermi level decreases, the conductance increases, suggesting that the LUMO is responsible for the conductance. As mentioned above, the HOMO-like states are much farther away from the Fermi level and cannot contribute to the conductance significantly. This is further supported by the results with the negative voltage, where the Fermi level came closer to the HOMO level but the conductance still decreased. Besides, the shape of the LDOS plot for the states near the Fermi level (Figure 6b) resembles that of the LDOS plot for the LUMO state of the isolated TFTPA molecule, while the HOMO state was mainly localized on the benzene ring.

CONCLUSIONS

We report the formation of an ordered layer of TFTPA on a negatively charged Au(111) using EC-STM followed by conductance measurements of single TFTPA molecules through the STM-BJ method. STM images revealed an ordered adlayer, likely formed by hydrogen bonding between carboxylic acids as well as halogen−halogen interactions of neighboring TFTPA molecules, with the benzene ring lying flat on Au(111). This orientation facilitates the direct π binding of the TFTPA benzene ring to the electrodes. Considering the amount of lateral drift between approach−retract cycles, the tip will not land back on the same spot. In addition, each molecule is surrounded by neighboring molecules, hence its flat orientation is stabilized through the existence of the hydrogen bonding network. Therefore, the molecular geometry in the junction remains quasi-flat during the break junction process. The measured conductance values for TFTPA and TPA, 0.24 and 0.22 G_0, respectively, perpendicular to the molecule plane are 3 orders of magnitude higher than through single-molecule junctions formed by benzene derivatives attached to electrodes

DOI: 10.1021/jacs.9b05448
J. Am. Chem. Soc. 2019, 141, 10109−10116

via anchoring groups, semiquantitatively agreeing with the nonequilibrium Green's function calculation. (Deviations between experiment and calculation are discussed in detail in the Supporting Information.) Molecules oriented flat on the electrode surface forming single-molecule junctions with no involvement of anchoring groups have a shorter tunneling barrier and higher conductance values. The tunneling process is dominated by the LUMO orbital of TFTPA and TPA according to the observed trend in conductance at different sample potentials and first-principles computation.

■ ASSOCIATED CONTENT

Supporting Information

The Supporting Information is available free of charge on the ACS Publications website at DOI: 10.1021/jacs.9b05448.

Chemicals and solutions, STM cell setup and sample preparation, electrochemical scanning tunneling microscopy imaging, electrochemical scanning tunneling microscopy break junction measurement, detailed analysis of STM images of TFTPA, sample rejected current−distance curves, single-molecule conductance vs sample bias, single molecule conductance vs sample potential, detailed analysis of STM images of TPA, single-molecule conductance control experiments, and computational details (PDF)

■ AUTHOR INFORMATION

Corresponding Author

*eborguet@temple.edu

ORCID

Parisa Yasini: 0000-0001-8072-6597

Author Contributions

§These authors contributed equally.

Notes

The authors declare no competing financial interest.

■ ACKNOWLEDGMENTS

The authors thank Nima Khaki for the design of the TOC and STM-BJ model figures. P.Y. and E.B. acknowledge Dr. Zhihai Li from Ball State University, Dr. Manuel Smeu from Binghamton University, and Dr. Tim Albrecht from Birmingham University for useful discussions. This work was supported by funding from the National Science Foundation (CHE-1508567) and as part of the Center for the Computational Design of Functional Layered Materials (CCDM) and The Center for Complex Materials from First-Principles (CCM), an Energy Research Center funded by the U.S. Department of Energy, Office of Science, Basic Energy Sciences, under grant no. DE-SC0012575.

■ REFERENCES

(1) Song, H.; Reed, M. A.; Lee, T. Single Molecule Electronic Devices. *Adv. Mater.* **2011**, *23*, 1583−1608.

(2) Komoto, Y.; Fujii, S.; Iwane, M.; Kiguchi, M. Single-molecule junctions for molecular electronics. *J. Mater. Chem. C* **2016**, *4*, 8842−8858.

(3) He, Y.; Borguet, E. Dynamics of Porphyrin Electron-Transfer Reactions at the Electrode−Electrolyte Interface at the Molecular Level. *Angew. Chem., Int. Ed.* **2007**, *46*, 6098−6101.

(4) Tao, N. J. Probing Potential-Tuned Resonant Tunneling through Redox Molecules with Scanning Tunneling Microscopy. *Phys. Rev. Lett.* **1996**, *76*, 4066−4069.

(5) Li, Z.; Smeu, M.; Rives, A.; Maraval, V.; Chauvin, R.; Ratner, M. A.; Borguet, E. Towards graphyne molecular electronics. *Nat. Commun.* **2015**, *6*, 6321.

(6) Baghernejad, M.; Manrique, D. Z.; Li, C.; Pope, T.; Zhumaev, U.; Pobelov, I.; Moreno-Garcia, P.; Kaliginedi, V.; Huang, C.; Hong, W.; Lambert, C.; Wandlowski, T. Highly-Effective Gating of Single-Molecule Junctions: An Electrochemical Approach. *Chem. Commun.* **2014**, *50*, 15975−15978.

(7) Vezzoli, A.; Grace, I.; Brooke, C.; Wang, K.; Lambert, C. J.; Xu, B.; Nichols, R. J.; Higgins, S. J. Gating of single molecule junction conductance by charge transfer complex formation. *Nanoscale* **2015**, *7*, 18949−18955.

(8) Komoto, Y.; Isshiki, Y.; Fujii, S.; Nishino, T.; Kiguchi, M. Evaluation of the Electronic Structure of Single-Molecule Junctions Based on Current-Voltage and Thermopower Measurements: Application to C-60 Single-Molecule Junction. *Chem. - Asian J.* **2017**, *12*, 440−445.

(9) Huang, M.-J.; Hsu, L.-Y.; Fu, M.-D.; Chuang, S.-T.; Tien, F.-W.; Chen, C.-h. Conductance of Tailored Molecular Segments: A Rudimentary Assessment by Landauer Formulation. *J. Am. Chem. Soc.* **2014**, *136*, 1832−1841.

(10) Kiguchi, M.; Murakoshi, K. Highly Conductive Single Molecular Junctions by Direct Binding of π-Conjugated Molecule to Metal Electrodes. *Thin Solid Films* **2009**, *518*, 466−469.

(11) Kaneko, S.; Nakazumi, T.; Kiguchi, M. Fabrication of a Well-Defined Single Benzene Molecule Junction Using Ag Electrodes. *J. Phys. Chem. Lett.* **2010**, *1*, 3520−3523.

(12) Afsari, S.; Li, Z.; Borguet, E. Orientation-Controlled Single-Molecule Junctions. *Angew. Chem., Int. Ed.* **2014**, *53*, 9771−9774.

(13) Komoto, Y.; Fujii, S.; Nishino, T.; Kiguchi, M. High Electronic Couplings of Single Mesitylene Molecular Junctions. *Beilstein J. Nanotechnol.* **2015**, *6*, 2431−2437.

(14) Kaneko, S.; Motta, C.; Brivio, G. P.; Kiguchi, M. Mechanically controllable bi-stable states in a highly conductive single pyrazine molecular junction. *Nanotechnology* **2013**, *24*, 315201.

(15) Mine, M.; Tsutsui, T.; Miyoshi, E. Theoretical Study on the Conductance of Benzene Clusters in the pi-Stack Direction. *Jpn. J. Appl. Phys.* **2008**, *47*, 8033−8038.

(16) Wang, H.; Jiang, Z. L.; Wang, Y. F.; Sanvito, S.; Hou, S. M. Quantitative Interpretation of the Low-Bias Conductance of Au-Mesitylene-Au Molecular Junctions Formed from Mesitylene Monolayers. *ChemPhysChem* **2016**, *17*, 2272−2277.

(17) Tanimoto, S.; Tsutsui, M.; Yokota, K.; Taniguchi, M. Dipole Effects on the Formation of Molecular Junctions. *Nanoscale Horiz.* **2016**, *1*, 399−406.

(18) Park, Y. S.; Widawsky, J. R.; Kamenetska, M.; Steigerwald, M. L.; Hybertsen, M. S.; Nuckolls, C.; Venkataraman, L. Frustrated Rotations in Single-Molecule Junctions. *J. Am. Chem. Soc.* **2009**, *131*, 10820−10821.

(19) Kiguchi, M.; Miura, S.; Hara, K.; Sawamura, M.; Murakoshi, K. Conductance of a single molecule anchored by an isocyanide substituent to gold electrodes. *Appl. Phys. Lett.* **2006**, *89*, 213104.

(20) Chen, F.; Li, X.; Hihath, J.; Huang, Z.; Tao, N. Effect of Anchoring Groups on Single-Molecule Conductance: Comparative Study of Thiol-, Amine-, and Carboxylic-Acid-Terminated Molecules. *J. Am. Chem. Soc.* **2006**, *128*, 15874−15881.

(21) Venkataraman, L.; Klare, J. E.; Tam, I. W.; Nuckolls, C.; Hybertsen, M. S.; Steigerwald, M. L. Single-Molecule Circuits with Well-Defined Molecular Conductance. *Nano Lett.* **2006**, *6*, 458−462.

(22) Chen, F.; Peng, L.-L.; Hong, Z.-W.; Mao, J.-C.; Zheng, J.-F.; Shao, Y.; Niu, Z.-J.; Zhou, X.-S. Comparative Study on Single-Molecule Junctions of Alkane- and Benzene-Based Molecules with Carboxylic Acid/Aldehyde as the Anchoring Groups. *Nanoscale Res. Lett.* **2016**, *11*, 380.

(23) Li, Z.; Han, B.; Wan, L.; Wandlowski, T. Supramolecular nanostructures of 1,3,5-benzene-tricarboxylic acid at electrified au(111)/0.05 M H_2SO_4 interfaces: An in situ scanning tunneling microscopy study. *Langmuir* **2005**, *21*, 6915−6928.

DOI: 10.1021/jacs.9b05448
J. Am. Chem. Soc. 2019, 141, 10109−10116

(24) Aitchison, H.; Lu, H.; Hogan, S.; Fruchtl, H.; Cebula, I.; Zharnikov, M.; Buck, M. Self-Assembled Monolayers of Oligophenylenecarboxylic Acids on Silver Formed at the Liquid-Solid Interface. *Langmuir* **2016**, *32*, 9397−9409.
(25) Su, G. J.; Zhang, H. M.; Wan, L. J.; Bai, C. L.; Wandlowski, T. Potential-induced phase transition of trimesic acid adlayer on Au(111). *J. Phys. Chem. B* **2004**, *108*, 1931−1937.
(26) He, Y.; Ye, T.; Borguet, E. The role of hydrophobic chains in self-assembly at electrified interfaces: Observation of potential-induced transformations of two-dimensional crystals of hexadecane by in-situ scanning tunneling microscopy. *J. Phys. Chem. B* **2002**, *106*, 11264−11271.
(27) Cavallo, G.; Metrangolo, P.; Milani, R.; Pilati, T.; Priimagi, A.; Resnati, G.; Terraneo, G. The Halogen Bond. *Chem. Rev.* **2016**, *116*, 2478−2601.
(28) Bosch, E.; Barnes, C. L. Triangular Halogen-Halogen-Halogen Interactions as a Cohesive Force in the Structures of Trihalomesitylenes. *Cryst. Growth Des.* **2002**, *2*, 299−302.
(29) He, Y.; Borguet, E. Dynamics of metastable nanoscale island growth and dissolution at electrochemical interfaces by time-resolved scanning tunneling microscopy. *J. Phys. Chem. B* **2001**, *105*, 3981−3986.
(30) Lipkowski, J.; Stolberg, L.; Yang, D.; Pettinger, B.; Mirwald, S.; Henglein, F.; Kolb, D. Molecular Adsorption at Metal-Electrodes. *Electrochim. Acta* **1994**, *39*, 1045−1056.
(31) Cuesta, A.; Kleinert, M.; Kolb, D. M. The adsorption of sulfate and phosphate on Au(111) and Au(100) electrodes: an in situ STM study. *Phys. Chem. Chem. Phys.* **2000**, *2*, 5684−5690.
(32) Kondo, T.; Morita, J.; Hanaoka, K.; Takakusagi, S.; Tamura, K.; Takahasi, M.; Mizuki, J. i.; Uosaki, K. Structure of Au(111) and Au(100) Single-Crystal Electrode Surfaces at Various Potentials in Sulfuric Acid Solution Determined by In Situ Surface X-ray Scattering. *J. Phys. Chem. C* **2007**, *111*, 13197−13204.
(33) Jewell, A.; Tierney, H.; Sykes, E. Gently lifting gold's herringbone reconstruction: Trimethylphosphine on Au(111). *Phys. Rev. B: Condens. Matter Mater. Phys.* **2010**, *82*, 205401.
(34) He, Y. F.; Borguet, E. Metastable Phase of the Au(111) Surface in Electrolyte Revealed by STM and Asymmetric Potential Pulse Perturbation. *J. Phys. Chem. C* **2011**, *115*, 5726−5731.
(35) Kroger, J.; Jensen, H.; Berndt, R. Conductance of tip-surface and tip-atom junctions on Au(111) explored by a scanning tunnelling microscope. *New J. Phys.* **2007**, *9*, 153.
(36) Xu, B.; Tao, N. J. Measurement of Single-Molecule Resistance by Repeated Formation of Molecular Junctions. *Science* **2003**, *301*, 1221.
(37) Capozzi, B.; Low, J. Z.; Xia, J.; Liu, Z.-F.; Neaton, J. B.; Campos, L. M.; Venkataraman, L. Mapping the Transmission Functions of Single-Molecule Junctions. *Nano Lett.* **2016**, *16*, 3949−3954.
(38) Sayed, S.; Fereiro, J.; Yan, H.; McCreery, R.; Bergren, A. Charge transport in molecular electronic junctions: Compression of the molecular tunnel barrier in the strong coupling regime. *Proc. Natl. Acad. Sci. U. S. A.* **2012**, *109*, 11498−11503.
(39) Nitzan, A.; Ratner, M. Electron transport in molecular wire junctions. *Science* **2003**, *300*, 1384−1389.
(40) Sun, L.; Diaz-Fernandez, Y.; Gschneidtner, T.; Westerlund, F.; Lara-Avila, S.; Moth-Poulsen, K. Single-molecule electronics: from chemical design to functional devices. *Chem. Soc. Rev.* **2014**, *43*, 7378−7411.
(41) Su, T.; Neupane, M.; Steigerwald, M.; Venkataraman, L.; Nuckolls, C. Chemical principles of single-molecule electronics. *Nat. Rev. Mater.* **2016**, *1*, 16002.
(42) Reecht, G.; Lotze, C.; Sysoiev, D.; Huhn, T.; Franke, K. Visualizing the Role of Molecular Orbitals in Charge Transport through Individual Diarylethene Isomers. *ACS Nano* **2016**, *10*, 10555−10562.
(43) Venkataraman, L.; Park, Y. S.; Whalley, A. C.; Nuckolls, C.; Hybertsen, M. S.; Steigerwald, M. L. Electronics and Chemistry: Varying Single-Molecule Junction Conductance Using Chemical Substituents. *Nano Lett.* **2007**, *7*, 502−506.
(44) Han, B.; Li, Z.; Wandlowski, T. Adsorption and self-assembly of aromatic carboxylic acids on Au/electrolyte interfaces. *Anal. Bioanal. Chem.* **2007**, *388*, 121−129.
(45) Sun, Y.-Y.; Peng, Z.-L.; Hou, R.; Liang, J.-H.; Zheng, J.-F.; Zhou, X.-Y.; Zhou, X.-S.; Jin, S.; Niu, Z.-J.; Mao, B.-W. Enhancing electron transport in molecular wires by insertion of a ferrocene center. *Phys. Chem. Chem. Phys.* **2014**, *16*, 2260−2267.
(46) Kitaguchi, Y.; Habuka, S.; Okuyama, H.; Hatta, S.; Aruga, T.; Frederiksen, T.; Paulsson, M.; Ueba, H. Controlling Single-Molecule Junction Conductance by Molecular Interactions. *Sci. Rep.* **2015**, *5*, 11796.
(47) Papior, N.; Lorente, N.; Frederiksen, T.; Garcia, A.; Brandbyge, M. Improvements on non-equilibrium and transport Green function techniques: The next-generation TRANSIESTA. *Comput. Phys. Commun.* **2017**, *212*, 8−24.
(48) Papior, N.; Gunst, T.; Stradi, D.; Brandbyge, M. Manipulating the voltage drop in graphene nanojunctions using a gate potential. *Phys. Chem. Chem. Phys.* **2016**, *18*, 1025−1031.

DOI: 10.1021/jacs.9b05448
J. Am. Chem. Soc. 2019, 141, 10109−10116